ChemPubSoc Europe

DOI: 10.1002/chem.201304826

CHEMISTRY A European Journal Full Paper

Cluster Compounds

Hydroxo-Bridged Dimers of Oxo-Centered Ruthenium(III) Triangle: Synthesis and Spectroscopic and Theoretical Investigations

Apoorva Upadhyay,[a] Jitendrasingh Rajpurohit,[a] Mukesh Kumar Singh,[a] Richa Dubey,[b] Anant Kumar Srivastava,[c] Ashutosh Kumar,[b] Gopalan Rajaraman,*[a] and Maheswaran Shanmugam*[a]

Abstract: The homometallic hexameric ruthenium cluster of the formula $[Ru^{III}_6(\mu_3\text{-}O)_2(\mu\text{-}OH)_2((CH_3)_3CCO_2)_{12}(py)_2]$ (**1**) (py = pyridine) is solved by single-crystal X-ray diffraction. Magnetic susceptibility measurements performed on **1** suggest that the antiferromagnetic interaction between the Ru^{III} centers is dominant, and this is supported by theoretical studies. Theoretical calculations based on density functional methods yield eight different exchange interaction values for **1**: $J_1 = -737.6$, $J_2 = +63.4$, $J_3 = -187.6$, $J_4 = +124.4$, $J_5 = -376.4$, $J_6 = -601.2$, $J_7 = -657.0$, and $J_8 = -800.6\ cm^{-1}$. Among all the computed J values, six are found to be antiferromagnetic. Four exchange values (J_1, J_6, J_7 and J_8) are computed to be extremely strong, with J_8, mediated through one μ-hydroxo and a carboxylate bridge, being by far the largest exchange obtained for any transition-metal cluster. The origin of these strong interactions is the orientation of the magnetic orbitals in the Ru^{III} centers, and the computed J values are rationalized by using molecular orbital and natural bond order analysis. Detailed NMR studies (^1H, ^{13}C, HSQC, NOESY, and TOCSY) of **1** (in $CDCl_3$) confirm the existence of the solid-state structure in solution. The observation of sharp NMR peaks and spin-lattice time relaxation (T1 relaxation) experiments support the existence of strong intramolecular antiferromagnetic exchange interactions between the metal centers. A broad absorption peak around 600–1000 nm in the visible to near-IR region is a characteristic signature of an intracluster charge-transfer transition. Cyclic voltammetry experiments show that there are three reversible one-electron redox couples at −0.865, +0.186, and +1.159 V with respect to the Ag/AgCl reference electrode, which corresponds to two metal-based one-electron oxidations and one reduction process.

Introduction

Several oxo-centered trinuclear transition-metal clusters with the general formula $[M_3(\mu_3\text{-}O)(\mu\text{-}RCO_2)_6(L)_3]^{n+}$ (M^{n+} = Cr, Mn, Fe, and Ru) have been investigated over several decades with regard to their specific electronic, magnetic, physical, and chemical properties.[1] Among others, the trinuclear oxo-centered ruthenium carboxylate clusters are of particular interest because of their versatile redox properties and photochemical activities.[2] The molecular systems displaying electron transfer and energy transfer have attracted great interest owing to their potential application in electronic devices such as logic gates, electrochromic displays, and heat-shielding materials.[3] Additionally, various ruthenium complexes (monomers, paddle-wheel dimers, oxo-centered mixed-valence trimers) are well known for their catalytic properties.[2d,4] Oxo-centered ruthenium triangles functionalized on an electrode surface act as an electrochemical biosensor probe for ligand–receptor binding to detect a variety of biomolecules such as proteins, DNA, enzymes, and so on.[5]

Furthermore, superior intramolecular electron-transfer properties have been observed for pyrazine, bipyridine, bipyrimidine, or phosphine derivatives of bridged oxo-centered ruthenium triangles.[6] Although oxo-centered trinuclear-based clusters have been proposed for various applications, there are no straightforward synthetic methods that yield pure crystals directly in a one-pot reaction. Column chromatography is often employed to purify the metal complex, which is both time-consuming and labor-intensive. Similarly, the electronic and magnetic properties have been studied extensively for paddle-wheel dimeric ruthenium complexes;[7,8] however, detailed reports on the magnetic properties of homometallic oligomeric structures such as oxo-centered ruthenium triangles or other higher oligomeric or dendrimeric ruthenium complexes are

[a] A. Upadhyay, J. Rajpurohit, M. Kumar Singh, Prof. Dr. G. Rajaraman, Prof. Dr. M. Shanmugam
Department of Chemistry, Indian Institute of Technology Bombay
Powai, Mumbai, Maharashtra 400 076 (India)
Fax: (+91) 22-2576-7152
E-mail: rajaraman@chem.iitb.ac.in
eswar@chem.iitb.ac.in

[b] R. Dubey, Prof. Dr. A. Kumar
Department of Biosciences and Bioengineering
Indian Institute of Technology Bombay
Powai, Mumbai, Maharashtra 400 076 (India)

[c] A. Kumar Srivastava
Department of Chemistry
Indian Institute of Science Education and Research
Pune, Maharashtra 411 008 (India)

Supporting information for this article is available on the WWW under http://dx.doi.org/10.1002/chem.201304826.

very limited in the literature.[7b,c] In this article, we report a novel one-pot synthetic route for the isolation of a homometallic trivalent hexameric cluster $[Ru_6(\mu_3\text{-}O)_2(\mu\text{-}OH)_2((CH_3)_3CCO_2)_{12}(py)_2]$ (**1**), which is purified solely by the solvent-extraction method. To the best of our knowledge, this is the first {Ru6} cluster in which two oxo-centered ruthenium triangles are connected by hydroxo bridges. The isolated complex is characterized by single-crystal X-ray diffraction, magnetic susceptibility measurements, spectroscopy (UV/Vis/NIR, NMR) cyclic voltammetry, and theoretical studies.

Results and Discussion

The reaction of ruthenium trichloride hydrate in an excess of pivalic acid ($(CH_3)_3CCO_2H$) in the presence of potassium hydroxide at elevated temperature gives the air- and moisture-stable hexameric ruthenium cluster of molecular formula $[Ru_6^{III}(\mu_3\text{-}O)_2((CH_3)_3CCO_2)_{12}(\mu\text{-}OH)_2(Py)_2]$ (**1**) (Py = Pyridine), which is characterized by X-ray crystallography (Figure 1). The crystal

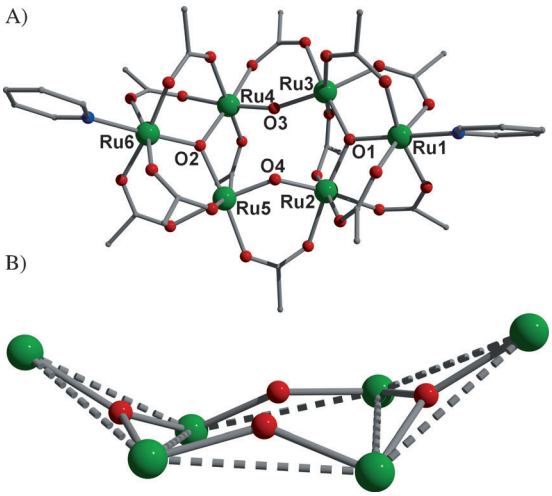

Figure 1. A) Ball-and-stick model representation of single-crystal X-ray diffraction structure of complex **1**. B) The metal core arrangement in **1** along with its oxo and hydroxo bridging units. Color code: Green = Ru^{III}, red = O, blue = N; grey = C. Side-chain carbon atoms and hydrogen atoms are omitted for clarity.

structure of **1** is solved in a monoclinic, $P2_1/n$ space group (Table 1). Structural analysis shows that there are two oxo-centered ruthenium triangles, (Ru1, Ru2, Ru3 and Ru4, Ru5, Ru6), which are bridged by two hydroxo ligands (O3 and O4) in a η^2 fashion. In addition to the hydroxo linkage, further links between the two triangles are provided by two carboxylate ligands. The remaining two edges of each ruthenium oxo-centered triangle are coordinated by four pivalate groups sharing two carboxylates for each edge.

The third edge of each triangle is linked by one carboxylate ligand, and the terminal coordination sites are completed by two pyridine ligands. All six ruthenium ions are in the trivalent oxidation state, and show distorted octahedral geometries with Ru^{III}–O bond lengths ranging from 1.826 to 2.086 Å, with the shortest bond length observed for the Ru^{III}–(μ-OH) group

Table 1. X-ray crystallographic data of complex **1**.

Formula	$C_{70}H_{120}O_{28}N_2Ru_6$
Size	0.15×0.13×0.08
System	Monoclinic
Space group	$P2_1/n$
a [Å]	24.31(2)
b [Å]	17.23(14)
c [Å]	24.43(2)
β [°]	112.121(2)
V [Å^3]	9485.3(14)
Z	4
ρ_{calcd} [g cm^{-1-3}]	1.460
$2\theta_{max}$ [°]	56.72
Radiation	$Mo_{K\alpha}$
λ [Å]	0.71073
T [K]	100
Reflns	141807
Ind. reflns	23649
reflns with $>2\sigma$(I)	16740
$R1$	0.0378
$wR2$	0.1035

(1.826 to 1.839 Å). A slightly longer distance was found between the Ru^{III}–μ_3-O groups (1.902 to 1.961 Å). The Ru^{III}–N bond lengths range from 2.110 to 2.115 Å. The observed bond lengths for the ruthenium ions are in the typical range of Ru^{III}–O and Ru^{III}–N bond lengths reported previously in the literature.[9]

Complex **1** is one of the largest carboxylate-based ruthenium clusters characterized by X-ray diffraction, unlike $[Ru_3O(RCO_2)_6(L)_x]$-derived dendrimeric structure units.[6b,e,10] Several dimers of oxo-centered ruthenium triangles are known, in which two Ru_3O units are bridged by pyrazine, bipyrimidine, bipyridine, and some phosphine-derivative ligands. However, linkage between the two Ru_3O cores provided by the hydroxo ligand (average Ru–OH = 1.832 Å) is reported here for the first time. This short linkage between the triangles could facilitate strong communication between the oxo-centered triangular units. Selected bond lengths and bond angles for **1** are given in Table S1 in the Supporting Information. All the ruthenium ions in the oxo-centered triangles are in-plane, but the triangles are non-coplanar. Although the triangular units in **1** appear to be analogous to each other, their structural parameters are slightly different (see Table S1). The metal core in **1** is arranged in a twisted boat conformation (see Figure 1 B). The majority of reported dimers, trimers, or oligomers of oxo-centered triangular unit employ solvent-bound oxo-centered triangles (example: $[Ru_3(O)(RCO_2)_6(L)_2(solvent)]^{n+}$) as a precursor, and column chromatography is often required to isolate the pure complex.[6e,11] However, the synthetic method developed here is a straightforward one-pot reaction in which the cluster of interest (**1**) is isolated by using simple precursors (ruthenium trichloride hydrate) without the need for column chromatography.

Variable-temperature DC magnetic susceptibility data were obtained for the polycrystalline sample of **1** between 2 and 300 K with an applied magnetic field of 1.0 kG (Figure 2). The room-temperature $\chi_M T$ value was found to be 0.96 cm^3 K mol^{-1},

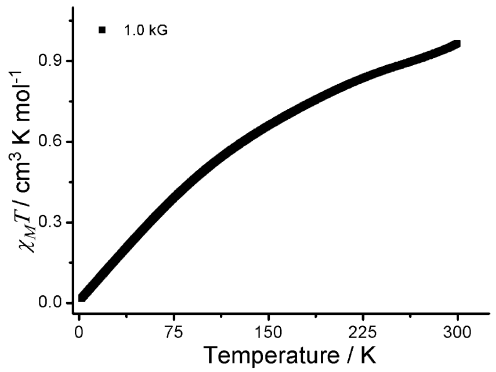

Figure 2. Variable-temperature DC magnetic susceptibility of polycrystalline sample of **1** measured at the indicated static field.

which is significantly lower than the expected spin-only value for six uncoupled Ru^{III} ions (low spin) (2.25 $cm^3 K mol^{-1}$, $g = 2.0$). A substantial variation in the room-temperature $\chi_M T$ value from the expected one indicates that antiferromagnetic interactions are dominant within complex **1** even at higher temperatures. The $\chi_M T$ value decreased further upon decreasing the temperature, and reached its final value of 0.03 $cm^3 K mol^{-1}$ at 2.0 K; this shows the predominant intramolecular antiferromagnetic interaction between the metal centers that leads to a singlet ground state in **1.**

Field-dependent magnetization measurements were performed for the powdered samples at various temperatures (Figure S1). Even at a high magnetic field (7.0 T) at various temperatures (2.0, 3.0, 5.0, 8.0, and 15.0 K), the magnetization value reaches a maximum value of 0.05–0.06 N μ_B. This scenario further supports the existence of a strong antiferromagnetic superexchange interaction between the metal centers in **1**.

To characterize the nature of the interaction between the metal centers, DFT calculations were performed on a model complex of **1**, in which the *t*-butyl groups are modeled as methyl to reduce the computational time required (see Figure 1 A). To begin with, the various spin states of Ru^{III} need to be properly addressed, as on many occasions, a combination of high-spin and low-spin $Ru^{(II/III)}$ has been employed in the literature to rationalize the metal–metal bonds.[12] We first performed calculations on a monomeric Ru^{III} model complex (see Figure S2) mimicking the coordination environment present in complex **1**, and our calculations suggest that $S = 1/2$ is the ground state, with the $S = 3/2$ and $S = 5/2$ states lying more than 200 kJ mol^{-1} higher in energy. This is consistent with the ligand-field paradigm, in which the 4d orbitals, owing to their large size and diffuse character, interact strongly with the ligands, leading to a low-spin configuration. Secondly, the $S = 1/2$ state is supposedly degenerate in a perfect octahedral environment; however, because of the distorted octahedral geometry present in this cluster, the ground state is found to be nondegenerate with the ground-state electronic configuration $(d_{xz})^2(d_{yz})^2(d_{xy})^1$, with the unpaired electron residing in the d_{xy} orbital. This is also consistent with the ligand-field paradigm proposed earlier.[13] As the ground state of the individual Ru^{III} has been clearly established, we then set out to compute the magnetic exchange between the neighboring Ru^{III} centers. A close inspection of the crystal structure suggests that all the $Ru^{III}\cdots Ru^{III}$ interactions are different, as they differ in either the Ru···Ru/Ru–O distances or Ru–O–Ru angles. Lists of structural parameters that are likely to influence the *J* values are given in Table 2. On the basis of the crystal structure parameters, an eight-*J* model was adopted for our computation (Figure 3). Our calculations yield the following parameters: $J_1 = -737.6$, $J_2 = +63.4$, $J_3 = -187.6$, $J_4 = +124.4$, $J_5 = -376.4$, $J_6 = -601.2$, $J_7 = -657.0$, and $J_8 = -800.6$ cm^{-1}. The J_1 and J_8 values are computed to be the second largest values reported for polynuclear transition-metal complexes; the recently reported {Fe^{II}-radical} complex is registered with the largest *J* value known to date.[14] Among the computed *J* values, J_1, J_3, J_5, J_6, J_7, and J_8 are computed to be antiferromagnetic, whereas the J_2 and J_4 interactions show moderate ferromagnetic coupling.

Table 2. Bridging groups between the paramagnetic Ru^{III} pairs and their important structural parameters based on X-ray diffraction.

	Bridging groups between Ru···Ru	Ru···Ru dist. [Å]	Ru–$O_{3/2}$–Ru [°]	Avg. Ru···$\mu_{3/2}$O [Å]
Ru1···Ru2 (J_1)	2{$(CH_3)_3CCO_2^-$}, μ_3-O^{2-}	3.343	119.8	1.932
Ru2···Ru3 (J_2)	{$(CH_3)_3CCOO^-$}, μ_3-O^{2-}	3.383	119.6	1.957
Ru1···Ru3 (J_3)	2{$(CH_3)_3CCOO^-$}, μ_3-O^{2-}	3.357	120.5	1.933
Ru4···Ru5 (J_4)	2{$(CH_3)_3CCOO^-$}, μ_3-O^{2-}	3.336	119.4	1.931
Ru5···Ru6 (J_5)	{$(CH_3)_3CCOO^-$}, μ_3-O^{2-}	3.380	119.1	1.960
Ru4···Ru6 (J_6)	2{$(CH_3)_3CCOO^-$}, μ_3-O^{2-}	3.369	121.5	1.931
Ru2···Ru5 (J_7)	{$(CH_3)_3CCOO^-$}, μ_2-OH^-	3.422	138.0	1.833
Ru3···Ru4 (J_8)	{$(CH_3)_3CCOO^-$}, μ_2-OH^-	3.420	138.0	1.831

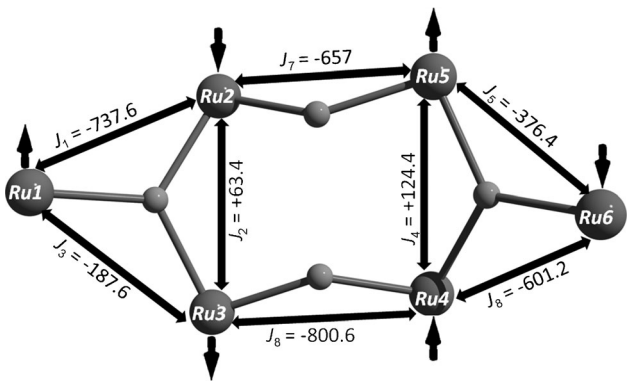

Figure 3. Adopted different magnetic coupling constants (J_1–J_8) based on molecular symmetry and crystal structure of **1**.

Among the computed J values, J_1, J_3, J_5 and J_6 are mediated by one μ_3-oxo and two carboxylate bridges, and J_2 and J_4 are mediated by one μ_3-oxo and one carboxylate bridge.

In contrast, the J_7 and J_8 interactions are mediated by a μ_2-OH bridge and one carboxylate bridge. Although structural variations for J_1–J_8 are noted for **1**, an initial look suggests that structural parameters alone cannot readily explain the variation in the J values, which span from $+124.4$ to -800.6 cm^{-1}.

To probe the origin of this interaction we analyzed the computed spin density and performed natural bond orbital (NBO) calculations. The computed spin density plot for the $S=3$ electronic spin state of **1** and the computed natural hybrid orbitals (NHO)[15] are shown in Figure 4 A and B, respectively. The d_{xy} orbitals of all the Ru^{III} centers are directed along the μ_3-oxo bridge. A closer look at the orbital orientation suggests that the d_{xy} orbitals of the Ru(1)–Ru(2) (J_1), Ru(4)–Ru(6) (J_6), Ru(2)–Ru(5) (J_7), and Ru(3)–Ru(4) (J_8) pairs are strongly interacting. This is also reflected in the computed overlap integral (S_{ab}) values for these exchange interactions, as large S_{ab} values are detected (Table S2).

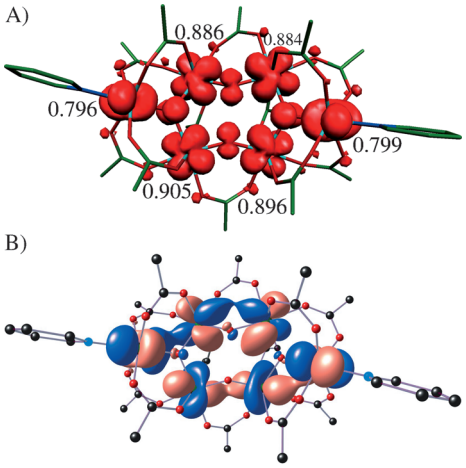

Figure 4. A) Spin-density plot of **1** with cutoff contour value of 0.005. B) NBO computed bonding interaction between Ru^{III} pairs in **1** with cutoff contour value of 0.047. The same labelling scheme has been followed for all Ru(III) as per in Figure 3.

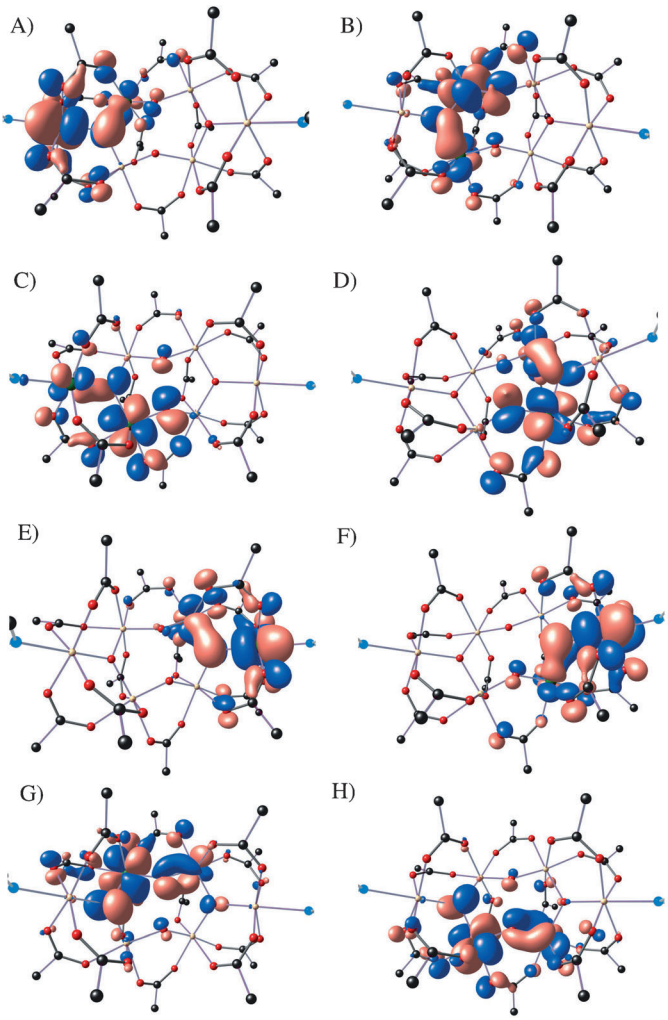

Figure 5. Molecular orbitals for all the J_1–J_8 (A–H, respectively) magnetic interactions. The same labelling scheme has been followed for all Ru(III) as per in Figure 3.

This helps to explain the strong antiferromagnetic J values computed for these pairs. The magnetic orbital of the J_1 interaction is shown in Figure 5 A. It is clear from this figure that this is a superexchange interaction as there are significant contributions to the SOMOs from both the μ_3-oxo and the carboxylate bridges. The d_{xy} orbital lies in the plane of the μ_3-oxo and two carboxylates, so exchange propagation through the carboxylate bridge is also facilitated. Thus, the magnetic exchange is found to propagate through all three bridges, leading to a strong antiferromagnetic J_1 interaction. For the J_2 interaction (see Figure 5 B), the d_{xy} orbitals are orthogonal to each other, leading to a moderate ferromagnetic coupling; this is also reflected in the computed overlap integral. The J_3 interaction, on the other hand, has a significant interaction between the two d_{xy} orbitals, but here, the magnetic exchange is found to propagate through the μ_3-oxo and one carboxylate bridge, whereas the magnetic orbitals are orthogonal to the orbitals of the second carboxylate (see Figure 5 C), and thus, do not participate in the magnetic exchange pathway. This leads to a weaker antiferromagnetic interaction compared to J_1. The J_4 interaction (see Figure 5 D) is similar to the J_2 interaction, in which the two d_{xy} orbitals are orthogonal to each other. The magnitude of the J_4 ferromagnetic coupling is larger than the J_2 interaction; this is because of the bridging carboxylate, in which the (μ_3)O–Ru–O(carb) angle is slightly shorter than in the J_2 interaction. This large ferromagnetic coupling ($J_4 > J_2$) is also reflected in the computed S_{ab} values. Although both J_5 and J_3 interactions have similar structural motifs, the orientation of the d_{xy} orbital favors J_5, as here, both the carboxylates participate in the magnetic coupling (Figure 5 E). As far as the J_6 interaction is concerned, the orientation is similar to that of J_1; nevertheless, the interactions are slightly weaker owing to the slightly longer Ru–O(μ_3) distances (Figure 5 F). Both the J_7 and J_8 interactions are mediated through a μ_2-OH and a carboxylate bridge. The d_{xy} orbitals on both ends are interact signifi-

cantly, just like in J_1 and J_6 coupling, but the Ru–O(H) distances are extremely short compared to the Ru–O(μ_3) distances (see Table 2).

The short Ru–O distance is accompanied by large Ru–O(H)–Ru angles (138.0 vs. 119.8°), and this leads to a very strong antiferromagnetic coupling (see Figure 5G for J_7 and 5H for J_8). The significantly enhanced overlap for this pair is also nicely reflected in the computed overlap integral. The computed spin density for **1** is given in Table S3 along with the spin densities of each of the [Ru_2Ga_4] models (Figure S3, Table S4). All the Ru^{III} centers have spin densities in the range 0.79 to 0.90, reflecting the fact that Ru^{III} promotes strong spin delocalization. Generally, metal ions with $(t_{2g})^5$ configurations promote spin polarization;[16] on the other hand, a large chunk of spin density is detected on the μ_3-O and μ_2-OH groups, suggesting that the 4d orbitals are very diffuse and reach up to the oxygen p orbitals to promote strong spin delocalization. In addition, the large spin-density value at the coordinated atoms suggests that the magnetic exchange is superexchange in nature. The simulation of the magnetic susceptibility using the computed J values is shown in Figure S4 along with the computed energy-level diagram for the spin structure. An $S=0$ ground state was detected for complex **1**, with the first excited state $S=1$ 587 cm^{-1} higher in energy. The next excited state is at 1148 cm^{-1} suggesting that solely the population difference between the ground state $S=0$ and first excited state $S=1$ determines the magnetic susceptibility behavior. This observation is clearly supported by the DC susceptibility data (Figure 2), and explains qualitatively the significant deviation of the $\chi_M T$ value at room temperature from the expected spin-only value of **1**. Besides, the gap between the ground state and first excited state is the largest obtained so far through a superexchange interaction for any transition-metal/metal-radical system. The $S=1$ state is also well isolated from the other excited states owing to the strong magnetic coupling; this suggests the possibility of obtaining isolated spin states at room temperature for potential applications in molecular nanomagnets.[17]

The computed values do not yield a good fit with the magnetic susceptibility data obtained experimentally. This is because the magnetic data collected are extremely sensitive to small changes in the J values, and even a slight variation in the parameter set can yield a reasonable fit to the data. By reducing the number of interactions to just three—two within the triangle and one between the triangle (see Figure S5A)—and taking the average of the DFT-calculated J values as a starting point, a good fit to the magnetic data is obtained, as shown in Figure S5B. Although this is the best fit obtained with three different J values, there are also other sets of parameters that also reasonably fit the data; however, all the fits yield very large antiferromagnetic exchange interactions, supporting the fact that the magnetic exchanges present in these clusters are relatively large.

To this end, both the $Ru^{3+}\cdots Ru^{3+}$ distances (average 3.361 Å; longest Ru···Ru bond: between 3.3 and 3.60 Å[6e]) and the orientation of the magnetic orbitals indicate that the interaction is superexchange in nature. Of particular interest to the current estimate of magnetic coupling is the report of Lueken and co-workers, in which a magnetic coupling as large as ≥ 760 cm^{-1} was estimated for a chloride-bridged dinuclear Ru^{III} complex.[7c] Such a large exchange interaction for a cluster compound was witnessed previously for a {V_8} cluster ($J=+723.6$ cm^{-1}).[18] In **1**, however several such strong exchange interactions of this order are present, and this leads to the largest ground state–excited state gap reported for any complex. The reported J values are also the largest known for any ruthenium clusters reported to date. This large interaction is essentially caused by the diffused nature of the 4d orbitals of Ru^{III}, which imply a way to obtain an isolated ground state at room temperature.[19] This invariably suggests that the incorporation of Ru^{III} in cluster aggregation can help obtain an isolated ground state at room temperature.

The electrospray mass spectrometric study confirms the existence of the solid-state structure of **1** in solution, with the intense m/z value of 2044 corresponding to the molecular weight of **1** (Figure S6).

Several low-valent ruthenium carbonyl, nitrosyl and/or mixed-valent diamagnetic oxo-centered triangles have been characterized by NMR spectroscopy as well as X-ray diffraction.[6a,20] However, similar studies for paramagnetic complexes are relatively rare owing to the line broadening, in particular, for large oligomeric complexes such as **1**.[2d,e,3d,7a] To check whether the strong antiferromagnetic exchange interaction predicted in theoretical calculations is sufficient to observe NMR signals, we characterized **1** by recording ^1H and ^{13}C NMR in $CDCl_3$ at 298 K. The observed NMR signals were remarkably sharp, and the chemical shift for the pyridine protons (Figure 6) appeared in the usual range. However, the chemical shift of the *tert*-butyl group of various carboxylates in **1** are found to be distributed over a window of −0.3 to 2.77 ppm. Some carboxylate groups are shifted upfield and others downfield compared with their usual chemical shift positions (see below for further details). This could be caused partly by the low-symmetry nature of **1** (pseudo *C*-2 symmetry) and the unpaired electrons present in **1**. Similar instances have already been documented in the literature for paramagnetic oxo-centered ruthenium(III) acetate triangles.[6e,21]

In the aromatic region, three different multiplets (Figure 6B) with unequal intensity were observed, which are assigned to the *ortho* (8.7 ppm), *para* (8.09 ppm), and *meta* (7.22 ppm) protons of the pyridine rings (see Figure 6B). The unequal multiplets (particularly the *para* protons) indicate that the aromatic pyridine rings are inequivalent, emphasizing that structural distortions found in the solid-state structure of **1** are maintained in solution. However, this chemically distinct environment is not well resolved for the aliphatic carboxylate group, possibly owing to the small difference in chemical shifts of these nuclei. The influence of unpaired electrons on the NMR peaks, that is, peak broadening or disappearance, is minimal in the case of **1**; this is probably because of the rapid exchange of unpaired electrons between the Ru^{III} ions, or because the NMR nuclei are appreciably distant (five bonds away, see Scheme S1) from the paramagnetic centers. Such a scenario has already been witnessed in other paramagnetic complexes such as the {$Cr^{III}_7Co^{II}$} wheels reported by Winpenny and co-workers.[22]

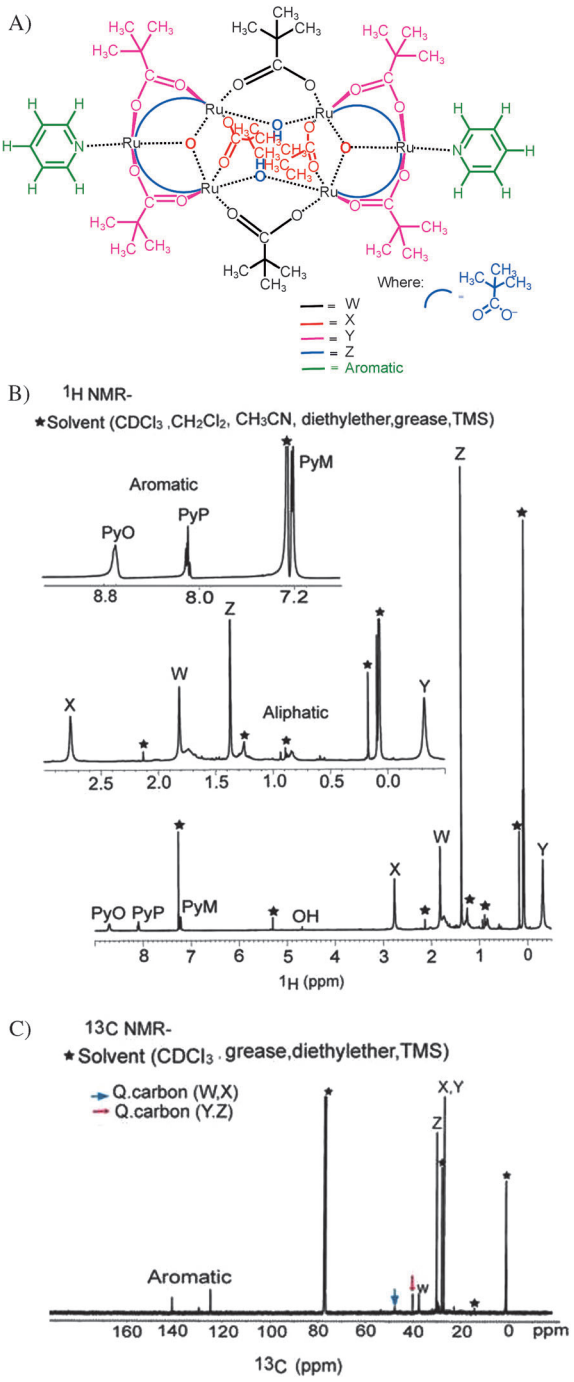

Figure 6. A) Schematic diagram of **1** highlighting the chemically equivalent ligated groups, which are represented in various colors with unique codes. The carboxylates projected toward the viewer (code: Y) lie above the triangular plane; the blue arch representing the other carboxylates (code: Z) lies below the triangular plane. B) ^{1}H NMR and C) ^{13}C NMR of **1** recorded in $CDCl_3$ at room temperature. Insets: Expanded aromatic and aliphatic region of ^{1}H NMR spectrum. ★ Represents residual solvent peaks acquired during purification and crystallization process.

In the aliphatic region of **1** (Figure 6B), there are four chemically distinct carboxylate groups (W, X, Y and Z; see Figure 6A for annotation of various groups), which are found in the range −0.3 to 2.77 ppm. Groups Y and Z correspond to eight carboxylate units: four of them (set Y) lie above the oxo-centered triangular plane, and the remaining ones (set Z) lie below the triangular plane. Sets W and X correspond to four carboxylates, of which two (set W) provide interlinkage between the two oxo-centered ruthenium triangles, and the other two (set X) establish intra linkage between two Ru^{III} ions within the triangle in each Ru_3O unit.

Among the *tert*-butyl protons of W, X, Y, and Z, protons classified under Y and Z show an upfield chemical shift compared with W and X. This scenario clearly reflects the fact that the protons of class Y and Z experience more electron density than those of class W and X. This observation agrees well with theoretical studies, in which it is predicted that the spin densities on Ru1 and Ru6 are significantly lower than those on the other Ru^{III} centers (Figure 4A), that is, the unpaired electrons present in these two atoms are significantly delocalized to atoms bound to them, directly influencing the chemical shifts of the protons. Between Y and Z, protons in class Y are shifted further upfield (−0.3 ppm), because the protons of Y are under the ring current of the pyridine. Again, this is strongly substantiated by the crystal structure: the class-Y protons are in a position to have a weak C–H···π interaction (Figure S7).[23] On the other hand, the group-W (1.84 ppm) and -X (2.77 ppm) protons are deshielded compared with Y and Z. Additionally, we observe a peak at 4.68 ppm, which can be assigned to the bridging hydroxo group in **1**. The assignment of these peaks was accomplished by using the bond-length (X-ray diffraction) parameters.

The spectral features observed in the ^{13}C NMR data are again consistent with the ^{1}H NMR data, in which the chemically distinct carboxylates (W, X, Y and Z) show a corresponding number of signals (Figure 6C). However, the *tert*-butyl groups of X and Y are merged to give one peak at 27.05 ppm (Figure 6C). The quaternary carbon atoms (arrow mark in Figure 6C) of these carboxylate groups are observed at 41.2 and 48.1 ppm. Taking into consideration their integral value, we assigned the peak at 41.2 ppm to Y, Z, and the peak at 48.1 ppm to W, X. Similarly, in the aromatic region, we observe three different signals, which are assigned to the *para* (124.9 ppm) and *ortho* (141.1 ppm and 129.7 ppm) carbon atoms of the pyridine rings. These assignments were made on the basis of the 2D ^{1}H-^{13}C HSQC spectrum (Figure 7). The distinct ^{13}C peak position for the *para* protons of the two pyridine rings reveals that the triangular units in **1** are chemically slightly different. The integration of the ^{1}H NMR signals is consistent with the expected number of various carboxylate groups and pyridine rings of a paramagnetic cluster (Table 3). Further, we performed various 2D experiments such as NOESY (Nuclear Overhauser Effect SpectroscopY), TOCSY (TOtal Correlation SpectroscopY), and ^{1}H-^{13}C HSQC (Heteronuclear Single Quantum Coherence) (Figure 7) to characterize **1** to the maximum extent. The correlations between the various aromatic protons are well established in the TOCSY spectrum (Figure 7D).

From the crystal structure, it is evident that the plane of the pyridine rings is tilted significantly from the ruthenium triangular plane. The non-coplanarity of these rings (with respect to the triangular plane) is even maintained in solution, as confirmed by the appearance of NOESY peaks (Figure 7B), that is,

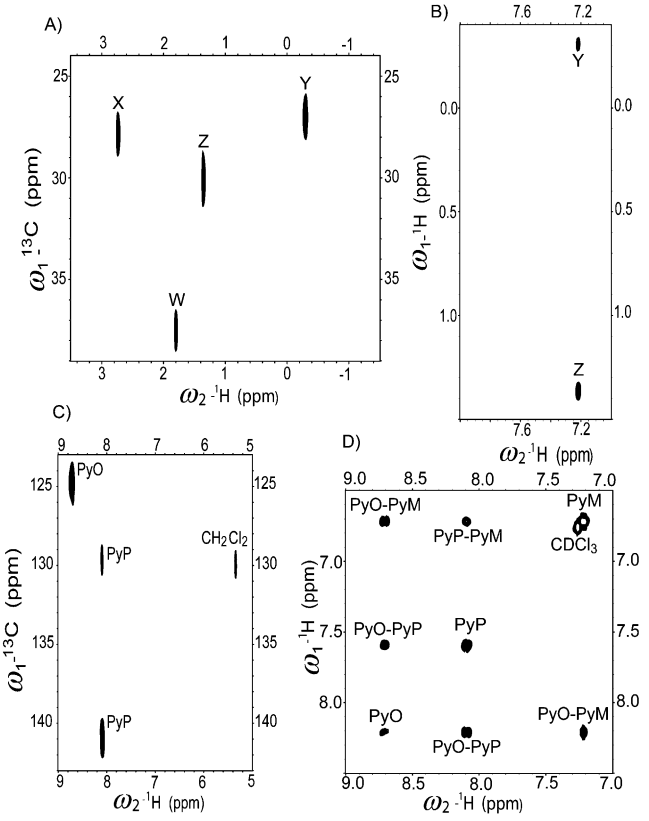

Figure 7. A, C) Excerpt from HSQC experiment showing various 1H-^{13}C correlations for **1**. Various ^{1}H-^{1}H correlations were extracted from B) the NOESY and D) the TOCSY experiments for **1**. W, X, Y, and Z represent the sets of carboxylates defined in Figure 6 A. PyO, PyM, and PyP represent the *ortho*, *meta*, and *para* protons of pyridine, respectively.

Table 3. Chemical shift assignments for ^{1}H and ^{13}C nuclei correlations extracted from HSQC experiment.

	^{1}H NMR	^{13}C NMR	Relative integral (for proton)
Pyridine(*ortho*)	8.7	124.9	1
Pyridine(*para*)	8.09	141.1	0.5818
	8.10	129.7	
Pyridine(*meta*)	7.22	–	0.9989
−OH	4.68	–	–
$-CH_3$ of Class X	2.77	27.05	4.48883
$-CH_3$ of Class W	1.84	37.55	4.9635
$-CH_3$ of Class Z	1.37	30.22	9.1531
$-CH_3$ of Class Y	-0.30	27.05	9.2140
Quaternary carbon (W, X)	–	48.1	–
Quaternary carbon (Y, Z)	-	41.2	-

the *meta* protons of both pyridine rings show a correlation with the methyl groups of Y and Z. This relates the spatial correlation of pyridine protons with the tertiary butyl group of carboxylates that are shorter than 5 Å, which is again consistent with the crystal structure of **1**. To find out the class of protons (W, X, Y, Z, or aromatic) that relaxes much faster because of the close proximity of an unpaired electron, we performed spin-lattice time-relaxation (T1) experiments at different temperatures. From the T1 relaxation experiments (Figure 8), we

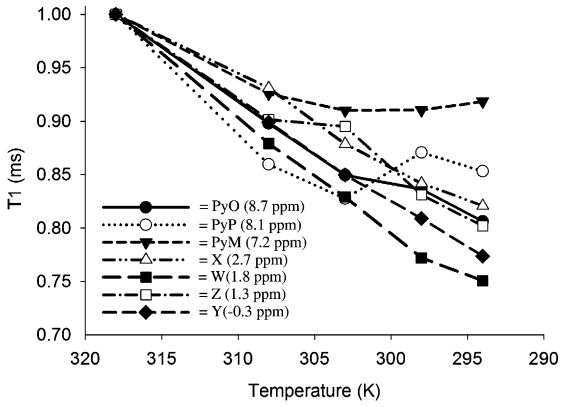

Figure 8. Spin-lattice relaxation time (T1 relaxation) measured at various temperatures.

noticed that, of the four groups (W, X, Y, and Z), the two sets of carboxylates W and Y showed relatively faster T1decay, suggesting that these could be closer to the paramagnetic center. In other words, the class-W and -Y protons appear to be relatively closer to the unpaired electron, which triggers faster relaxation, than those of the other carboxylates in **1**. Moreover, the line widths of the ^{1}H NMR signals were analyzed in detail; except for the class-Y protons (line width: 16 Hz at −0.3 ppm), all the signals were sharp. Presumably, this is because of the large spin density on the ligated atoms of Y bound to Ru1 and Ru6, which is again consistent with the spin-density distribution estimated from the theoretical calculations. The observed line width is significantly smaller than that for the other paramagnetic oxo-centered ruthenium(III) triangle (line width ≈200 Hz).[21a] Overall, the findings from the NMR experiments support indirectly and correlate strongly with the theoretical prediction of the large superexchange interaction (*J*) values for **1**.

The UV/Vis/NIR spectrum for **1** in dichloromethane is shown in Figure 9. Complex **1** shows a broad band around 600–1000 nm, and in the UV region, peaks of high intensity around 377, 228, and 275 nm.

A high-energy absorption band in the UV region (228 nm, $\varepsilon = 2.29\times10^5$ mol^{-1} cm^{-1}, and 275 nm, $\varepsilon = 1.04\times10^5$ mol^{-1} cm^{-1})

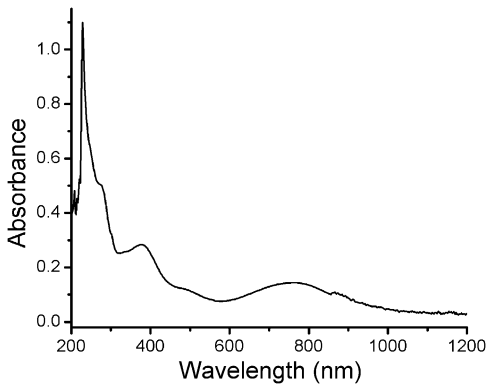

Figure 9. UV/Vis/NIR spectrum of 4.8×10^{-6} M concentration of **1** recorded in dichloromethane at room temperature.

is assigned as a ligand-based charge-transfer transition.[6b,e,10a,24] The absorption band observed at 300–400 nm ($\varepsilon = 5.87 \times 10^4\ mol^{-1}\,cm^{-1}$) is likely to be a cluster-to-ligand charge-transfer (CLCT) transition from the occupied dπ orbitals of the {Ru_3O} core to the π^* orbital of the terminal pyridine ligand.[2b,25] The broad band observed in the visible to near-infrared region (600–1000 nm, $\varepsilon = 2.98 \times 10^3\ mol^{-1}\,cm^{-1}$) could be attributed to the intracluster (IC) transition, which is a characteristic signature of the Ru_3O core in the cluster.[2b,6e] The position of this low-energy band is highly dependent on the number of valence d electrons available within the cluster, as has been the case for other mixed-valence systems reported elsewhere.[6d,25]

To check whether other possible redox states (changing the number of d electrons in **1**) can be attained for **1**, we performed cyclic voltammetry (CV) and differential pulse voltammetry (DPV) experiments in dry DCM, using a glassy-carbon electrode, a platinum auxiliary electrode, and an Ag/AgCl reference electrode. Tetrabutylammonium perchlorate was used as a supporting electrolyte. The cyclic voltammogram of **1** shows three reversible one-electron redox process at −0.865, +0.186, and +1.159 V (Figure 10), which correspond to metal-based

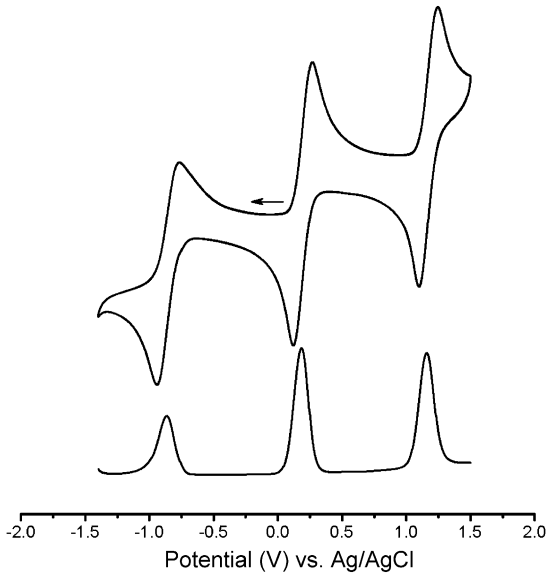

Figure 10. Cyclic voltammogram (top) and differential pulse voltammogram (bottom) of **1** (1×10^{-3} mol) recorded in dry CH_2Cl_2 using 0.1 M tetrabutylammonium perchlorate as a supporting electrolyte at a scan rate of 100 mV s^{-1}. The redox potentials are referenced to a Ag/AgCl electrode.

redox processes. The reduction at −0.865 V is assigned as $Ru_3^{III,III,III}\cdots Ru_3^{III,III,III}/Ru_3^{III,III,III}\cdots Ru_3^{III,III,II}$ and the other two consecutive oxidation processes at +0.186 V and +1.159 V are assigned as $Ru_3^{IV,III,III}\cdots Ru_3^{III,III,III}/Ru_3^{III,III,III}\cdots Ru_3^{III,III,III}$ and $Ru_3^{IV,III,III}\cdots Ru_3^{IV,III,III}/Ru_3^{IV,III,III}\cdots Ru_3^{III,III,III}$, respectively.[25] By exploiting the donor–acceptor property of the terminal or the bridging ligand, various oxidation states of the metal ion can be stabilized. This has already been witnessed in related structures (like **1**) reported elsewhere.[2b,d] We are currently investigating possible ways of stabilizing the various oxidation states of **1** to isolate the mixed-valent analogue of this cluster.

Conclusion

We have developed a one-pot synthetic method, which is free of chromatographic techniques, to isolate **1** in moderate yield. To the best of our knowledge, oxo-centered triangles with hydroxo bridging units are reported for the first time, and to date, complex **1** is one of the largest carboxylate-based ruthenium clusters known. Magnetic susceptibility data suggest that dominant intramolecular antiferromagnetic interactions between the metal centers lead to a diamagnetic ground state. The extent and origin of these superexchange interactions have been explained qualitatively on the basis of structural parameters, and predominantly, by the orientation of the magnetic orbitals. Detailed magnetic studies have been presented for the first time in a large oligomer such as **1**. The exchange interactions (J_1 and J_8) computed for **1** are the second largest known for the transition-metal clusters reported to date. The presence of several such superexchange interactions keeps the excited states significantly far from the ground state, and this gap is again by far the largest known for any complex reported to date. This suggests a perceivable way to obtain an isolated ground state in polynuclear complexes. Mass spectrometry confirms the existence of **1** in solution, which is strongly supported by NMR and absorption spectroscopy. Cyclic voltammetry experiments show that there are three reversible redox processes based on the ruthenium ions. Although complex **1** is paramagnetic, the strong delocalization of spins leads to strong superexchange (antiferromagnetic) interactions, which keep the excited states significantly far from the diamagnetic ground state. The strongest exchange interaction at room temperature along with the possibility of isolating mixed-valent ruthenium complexes (either by chemical or electrochemical oxidation or reduction) will pave the way for the isolation of molecules with discrete non-diamagnetic ground spin states, which has been a longstanding interest in the molecular magnetism community. This work is currently in progress in our laboratory.

Experimental Section

All the reactions were carried out under aerobic conditions. Analytical-grade solvents and reagents were purchased from commercial sources (Alfa Aesar) and used without further purification. Elemental analyses (CHN) were performed on a Thermoquestmicro analyzer. Infrared spectra were collected for the solid samples using KBr pellets on a PerkinElmer FTIR spectrometer in the range 400–4000 cm^{-1}. Electronic spectra were recorded on a Varian UV/Vis/NIR spectrophotometer in the range 200–1600 nm at room temperature. ESI mass spectrometry was performed with a Q-TOF micromass (YA-105) spectrometer. Cyclic voltammetry experiments were performed with a CHI-620E series instrument. Single-crystal data were collected on a Bruker SMART Apex duo instrument ($Mo_{K\alpha}$, $\lambda = 0.71073$ Å). The selected crystals were mounted on the tip of a glass pin with Paratone-N oil and placed in the cold flow produced by an Oxford Cryo-cooling device. Complete hemi-

spheres of data were collected using ω and ϕ scans (0.3 Å, 16 s per frame). Integrated intensities were obtained with SAINT+ and corrected for absorption using SADABS. Structure solution and refinement was performed with the SHELX-package. The structures were solved by direct methods and completed by iterative cycles of ΔF syntheses and full-matrix least-squares refinement against F^2. CCDC 975334. Magnetic susceptibility measurements were obtained with a Squid-VSM Quantum Design SQUID magnetometer. Measurements were performed on polycrystalline samples, and magnetic data were corrected for the sample holder and diamagnetic contribution. The isolated crystals of **1** from acetonitrile were recrystallized again from DCM/CH_3CN (1:9), and the crystals obtained were used for NMR studies. All NMR experiments were performed on a Bruker Avance 500 MHz NMR spectrometer equipped with a double/triple resonance gradient probe at 298 K. Data were processed using Topspin 2.1 and analyzed with Sparky 3.114.[26] The compound (20 mg) was dissolved in $CDCl_3$ to record the 1D proton spectrum with 256 scans and 66 K data points, and the ^{13}C spectrum with 16 K scans and 64 K data points. For assignment of the protons attached to the carbon atoms, the ^{1}H-^{13}C HSQC spectrum[27] was recorded with (2048×256) data points and 16 scans. Further, 2D TOCSY (MLEV17 sequence)[28] with a mixing time of 75 ms and a NOESY experiment[29] with a mixing time of 400 ms were performed with 32 scans having (2048×512) data points. Further, spin-lattice relaxation time (T1 relaxation) measurements were performed at 294, 298, 303, 308, and 318 K and fitted to a single exponential to calculate the T1 values. DFT calculations were performed using the Gaussian 09[30] suite of programs. The B3LYP[31] functional along with relativistic effective-core potential LANL08f[32] was employed for the Ru atoms, and the rest of the elements were treated with Ahlrichs triple-zeta TZV[33] basis sets. The widely used BS-DFT (Noodlemann's Broken Symmetry)[34] approach was used to compute all J values (J_1–J_8). The employed exchange Hamiltonian for **1** is given below [Eq. (1)].

$$H = -J_1(S_1.S_2) - J_2(S_2.S_3) - J_3(S_1.S_3) - J_4(S_4.S_5) - J_5(S_5.S_6) - J_6(S_4.S_6) - J_7(S_2.S_5) - J_8(S_3.S_4) \quad (1)$$

Although magnetic exchange can be calculated on the full structure of **1**,[35] the broken-symmetry solutions did not converge to the desired solution, despite our repetitive attempts with many possible techniques. Thus, we adapted the diamagnetic substitution method, in which all atoms except the desired Ru^{III} pairs were replaced by diamagnetic Ga^{III} atoms.[36] The eight magnetic exchanges were thus estimated from eight different fictitious $\{Ru_2Ga_4\}$ models. Simulation of the magnetic susceptibility was performed with PHI software suite.[37]

Synthesis of 1

Ruthenium trichloride hydrate (1.0 g) was added to pivalic acid (20 mL) and the red–brown solution was stirred for 5 min. KOH (2.0 g) was added to this solution, and the reaction mixture was heated to 160 °C, giving a dark green solution. Heating was continued for 7 h with constant stirring. The temperature of the reaction mixture was reduced to 100 °C and the excess pivalic acid was removed by distillation under reduced pressure. H_2O (25.0 mL) was added to this residue to remove the salt impurities. The whole water suspension was transferred into a separating funnel. Diethylether (20 mL) was added to this suspension. The product of interest remains in the organic layer and other impurities are in the aqueous layer. The organic layer was washed two more times with water to ensure the complete removal of salt impurities. The organic layer was collected and rotary evaporation to dryness resulted in a green black mass. Acetonitrile (20 mL, added in portions) was added to this, and the resultant green solution was collected by filtration. Single crystals of X-ray quality were grown within 24 h upon addition of pyridine (1.0 mL) to the above acetonitrile solution, which was boiled for 2–3 min before being kept for crystallization. Yield: 110 mg (7%); elemental analysis calcd (%) for $C_{70}H_{120}O_{28}N_2Ru_6$: C 41.13, H 5.92, N 1.37; found: C 40.40, H 5.84, N 1.57; FTIR: $\tilde{\nu}$ = 2958 (w, ν_{Ar-H}), 1605 (w, $\nu_{C=N}$), 1069 (w, ν_{C-O}), 1557, 1483 cm^{-1} (s, ν_{COO}); ESI mass: m/z = 2044.

Acknowledgements

M.S. acknowledges DST (SR/S1/IC-32/2011), DST nanomission (SR/NM/NS-1119/2011) BRNS (2012/20/37C/12/BRNS) and IIT Bombay for financial support. G.R. acknowledges financial support from the Government of India through Department of Science and Technology (SR/S1/IC-41/2010, SR/NM/NS-1119/2011) and generous computational resources from the Indian Institute of Technology-Bombay. A.U. and M.K.S. thank CSIR and UGC, respectively, for their graduate fellowships. J.R. acknowledges IIT Bombay for a graduate fellowship.

Keywords: cluster compounds · density functional calculations · magnetism · NMR spectroscopy · ruthenium

[1] a) J. Ribas, B. Albela, H. Stoeckli-Evans, G. Christou, *Inorg. Chem.* **1997**, *36*, 2352–2360; b) R. Wu, M. Poyraz, F. E. Sowrey, C. E. Anson, S. Wocadlo, A. K. Powell, U. A. Jayasooriya, R. D. Cannon, T. Nakamoto, M. Katada, H. Sano, *Inorg. Chem.* **1998**, *37*, 1913–1921; c) I. S. Zavarine, C. P. Kubiak, T. Yamaguchi, K.-i. Ota, T. Matsui, T. Ito, *Inorg. Chem.* **2000**, *39*, 2696–2698; d) S. Maheswaran, G. Chastanet, S. J. Teat, T. Mallah, R. Sessoli, W. Wernsdorfer, R. E. P. Winpenny, *Angew. Chem.* **2005**, *117*, 5172–5176; *Angew. Chem. Int. Ed.* **2005**, *44*, 5044–5048; e) M. Shanmugam, G. Chastanet, T. Mallah, R. Sessoli, S. J. Teat, G. A. Timco, R. E. P. Winpenny, *Chem. Eur. J.* **2006**, *12*, 8777–8785; f) M. Shanmugam, M. Shanmugam, G. Chastanet, R. Sessoli, T. Mallah, W. Wernsdorfer, R. E. P. Winpenny, *J. Mater. Chem.* **2006**, *16*, 2576–2578.

[2] a) T. Ito, T. Hamaguchi, H. Nagino, T. Yamaguchi, J. Washington, C. Kubiak, *Science* **1997**, *277*, 660–663; b) H. E. Toma, C. J. Cunha, C. Cipriano, *Inorg. Chim. Acta* **1988**, *154*, 63–66; c) H. E. Toma, C. J. Cunha, *Can. J. Chem.* **1989**, *67*, 1632–1635; d) H. E. Toma, K. Araki, A. D. P. Alexiou, S. Nikolaou, S. Dovidauskas, *Coord. Chem. Rev.* **2001**, *219–221*, 187–234; e) J. A. Baumann, D. J. Salmon, S. T. Wilson, T. J. Meyer, W. E. Hatfield, *Inorg. Chem.* **1978**, *17*, 3342–3350; f) M. Itou, M. Otake, Y. Araki, O. Ito, H. Kido, *Inorg. Chem.* **2005**, *44*, 1580–1587; g) M. Otake, M. Itou, Y. Araki, O. Ito, H. Kido, *Inorg. Chem.* **2005**, *44*, 8581–8586; h) J.-L. Chen, L.-Y. Zhang, Z.-N. Chen, L.-B. Gao, M. Abe, Y. Sasaki, *Inorg. Chem.* **2004**, *43*, 1481–1490.

[3] a) L. F. O. Furtado, A. D. P. Alexiou, L. Goncalves, H. E. Toma, K. Araki, *Angew. Chem.* **2006**, *118*, 3215–3218; *Angew. Chem. Int. Ed.* **2006**, *45*, 3143–3146; b) Y. Tomiyasu, M. Abe, Y. Morihara, H. Ohgi, T. Otake, Y. Hisaeda, *Chem. Lett.* **2009**, *38*, 492–493; c) A. J. Göttle, I. M. Dixon, F. Alary, J.-L. Heully, M. Boggio-Pasqua, *J. Am. Chem. Soc.* **2011**, *133*, 9172–9174; d) F.-R. Dai, B. Li, L.-X. Shi, L.-Y. Zhang, Z.-N. Chen, *Dalton Trans.* **2009**, 10244–10249; e) B. J. Lear, C. P. Kubiak, *Inorg. Chem.* **2006**, *45*, 7041–7043.

[4] a) M. E. Harvey, D. G. Musaev, J. Du Bois, *J. Am. Chem. Soc.* **2011**, *133*, 17207–17216; b) S. Davis, R. S. Drago, *Inorg. Chem.* **1988**, *27*, 4759–4760; c) E. Ferrer Flegeau, C. Bruneau, P. H. Dixneuf, A. Jutand, *J. Am. Chem. Soc.* **2011**, *133*, 10161–10170; d) R. Cariou, C. Fischmeister, L. Toupet, P. H. Dixneuf, *Organometallics* **2006**, *25*, 2126–2128; e) P. B. Arockiam, C. Fischmeister, C. Bruneau, P. H. Dixneuf, *Angew. Chem.* **2010**,

122, 6779 – 6782; *Angew. Chem. Int. Ed.* **2010**, *49*, 6629 – 6632; f) S. A. Fouda, B. C. Y. Hui, G. L. Rempel, *Inorg. Chem.* **1978**, *17*, 3213 – 3220; g) C. A. Huff, J. W. Kampf, M. S. Sanford, *Organometallics* **2012**, *31*, 4643 – 4645.

[5] a) D. J. Feld, H.-T. Hsu, A. L. Eckermann, T. J. Meade, *Langmuir* **2012**, *28*, 939 – 949; b) R. N. Garner, J. C. Gallucci, K. R. Dunbar, C. Turro, *Inorg. Chem.* **2011**, *50*, 9213 – 9215; c) D. A. Lutterman, A. Chouai, Y. Liu, Y. Sun, C. D. Stewart, K. R. Dunbar, C. Turro, *J. Am. Chem. Soc.* **2008**, *130*, 1163 – 1170; d) A. Chouai, S. E. Wicke, C. Turro, J. Bacsa, K. R. Dunbar, D. Wang, R. P. Thummel, *Inorg. Chem.* **2005**, *44*, 5996 – 6003.

[6] a) J. C. Goeltz, C. P. Kubiak, *J. Am. Chem. Soc.* **2010**, *132*, 17390 – 17392; b) H. Ohtsu, N. Fujiwara, T. Yamaguchi, *Inorg. Chem.* **2011**, *50*, 7382 – 7384; c) J. A. Baumann, S. T. Wilson, D. J. Salmon, P. L. Hood, T. J. Meyer, *J. Am. Chem. Soc.* **1979**, *101*, 2916 – 2920; d) M. Abe, A. Inatomi, Y. Hisaeda, *Dalton Trans.* **2011**, *40*, 2289 – 2298; e) F.-R. Dai, Y.-H. Wu, L.-Y. Zhang, B. Li, L.-X. Shi, Z.-N. Chen, *Eur. J. Inorg. Chem.* **2011**, 2306 – 2316.

[7] a) H.-Y. Ye, F.-R. Dai, L.-Y. Zhang, Z.-N. Chen, *Inorg. Chem.* **2007**, *46*, 6129 – 6135; b) A. Ohto, Y. Sasaki, T. Ito, *Inorg. Chem.* **1994**, *33*, 1245 – 1246; c) U. Koelle, H. Lueken, K. Handrick, H. Schilder, J. K. Burdett, S. Balleza, *Inorg. Chem.* **1995**, *34*, 6273 – 6278.

[8] T. R. Weaver, T. J. Meyer, S. A. Adeyemi, G. M. Brown, R. P. Eckberg, W. E. Hatfield, E. C. Johnson, R. W. Murray, D. Untereker, *J. Am. Chem. Soc.* **1975**, *97*, 3039 – 3048.

[9] a) O. Almog, A. Bino, D. Garfinkel-Shweky, *Inorg. Chim. Acta* **1993**, *213*, 99 – 102; b) J. L. Chen, G. Q. Yin, Z. N. Chen, *Chin. Chem. Lett.* **2003**, *14*, 519 – 522; c) M. Abe, Y. Sasaki, T. Yamaguchi, T. Ito, *Bull. Chem. Soc. Jpn.* **1992**, *65*, 1585 – 1590.

[10] a) S. Nikolaou, D. M. Tomazela, M. N. Eberlin, H. E. Toma, *Transition Met. Chem.* **2008**, *33*, 1059 – 1065; b) S. D. Glover, J. C. Goeltz, B. J. Lear, C. P. Kubiak, *Coord. Chem. Rev.* **2010**, *254*, 331 – 345; c) K.-i. Ota, H. Sasaki, T. Matsui, T. Hamaguchi, T. Yamaguchi, T. Ito, H. Kido, C. P. Kubiak, *Inorg. Chem.* **1999**, *38*, 4070 – 4078.

[11] M. Abe, Y. Sasaki, Y. Yamada, K. Tsukahara, S. Yano, T. Yamaguchi, M. Tominaga, I. Taniguchi, T. Ito, *Inorg. Chem.* **1996**, *35*, 6724 – 6734.

[12] a) A. Das, T. K. Ghosh, A. Dutta Chowdhury, S. M. Mobin, G. K. Lahiri, *Polyhedron* **2013**, *52*, 1130 – 1137; b) K. M. Kadish, M. Nguyen, E. Van Caemelbecke, J. L. Bear, *Inorg. Chem.* **2006**, *45*, 5996 – 6003; c) M. Fabre, J. L. Jaud, M. Hliwa, J.-P. Launay, J. Bonvoisin, *Inorg. Chem.* **2006**, *45*, 9332 – 9345; d) S. Kannan, R. Ramesh, *Polyhedron* **2006**, *25*, 3095 – 3103; e) N. Sathya, P. Muthusamy, N. Padmapriya, G. Raja, K. Deivasigamani, C. Jayabalakrishnan, *J. Coord. Chem.* **2009**, *62*, 3532 – 3543; f) L. M. Toma, L. D. Toma, F. S. Delgado, C. Ruiz-Pacrez, J. Sletten, J. Cano, J. M. Clemente-Juan, F. Lloret, M. Julve, *Coord. Chem. Rev.* **2006**, *250*, 2176 – 2193.

[13] K. Meyer, E. Bill, B. Mienert, T. Weyhermueller, K. Wieghardt, *J. Am. Chem. Soc.* **1999**, *121*, 4859 – 4876.

[14] I.-R. Jeon, J. G. Park, D. J. Xiao, T. D. Harris, *J. Am. Chem. Soc.* **2013**, *135*, 16845 – 16848.

[15] J. P. Foster, F. Weinhold, *J. Am. Chem. Soc.* **1980**, *102*, 7211 – 7218.

[16] J. Cano, E. Ruiz, S. Alvarez, M. Verdaguer, *Comments Inorg. Chem.* **1998**, *20*, 27 – 56.

[17] a) R. J. Blagg, L. Ungur, F. Tuna, J. Speak, P. Comar, D. Collison, W. Wernsdorfer, E. J. L. McInnes, L. F. Chibotaru, R. E. P. Winpenny, *Nat. Chem.* **2013**, *5*, 673 – 678; b) R. Vincent, S. Klyatskaya, M. Ruben, W. Wernsdorfer, F. Balestro, *Nature* **2012**, *488*, 357 – 360; c) S.-Y. Lin, W. Wernsdorfer, L. Ungur, A. K. Powell, Y.-N. Guo, J. Tang, L. Zhao, L. F. Chibotaru, H.-J. Zhang, *Angew. Chem.* **2012**, *124*, 12939 – 12943; *Angew. Chem. Int. Ed.* **2012**, *51*, 12767 – 12771; d) M. Urdampilleta, N.-V. Nguyen, J.-P. Cleuziou, S. Klyatskaya, M. Ruben, W. Wernsdorfer, *Int. J. Mol. Sci.* **2011**, *12*, 6656 – 6667; e) Y.-N. Guo, G.-F. Xu, W. Wernsdorfer, L. Ungur, Y. Guo, J. Tang, H.-J. Zhang, L. F. Chibotaru, A. K. Powell, *J. Am. Chem. Soc.* **2011**, *133*, 11948 – 11951; f) A. Candini, S. Klyatskaya, M. Ruben, W. Wernsdorfer, M. Affronte, *Nano Lett.* **2011**, *11*, 2634 – 2639; g) W. Wernsdorfer, *Int. J. Nanotechnol.* **2010**, *7*, 497 – 522; h) M. Mannini, F. Pineider, C. Danieli, F. Totti, L. Sorace, P. Sainctavit, M. A. Arrio, E. Otero, L. Joly, J. C. Cezar, A. Cornia, R. Sessoli, *Nature* **2010**, *468*, 417 – 421; i) M. Mannini, F. Pineider, P. Sainctavit, C. Danieli, E. Otero, C. Sciancalepore, A. M. Talarico, M.-A. Arrio, A. Cornia, D. Gatteschi, R. Sessoli, *Nat. Mater.* **2009**, *8*, 194 – 197.

[18] K. Hegetschweiler, B. Morgenstern, J. Zubieta, P. J. Hagrman, N. Lima, R. Sessoli, F. Totti, *Angew. Chem.* **2004**, *116*, 3518 – 3521; *Angew. Chem. Int. Ed.* **2004**, *43*, 3436 – 3439.

[19] R. E. P. Winpenny, *J. Chem. Soc. Dalton Trans.* **2002**, 1 – 10.

[20] a) A. Inatomi, M. Abe, Y. Hisaeda, *Eur. J. Inorg. Chem.* **2009**, 4830 – 4836; b) J. C. Salsman, S. Ronco, C. H. Londergan, C. P. Kubiak, *Inorg. Chem.* **2006**, *45*, 547 – 554.

[21] a) J. C. Goeltz, C. J. Hanson, C. P. Kubiak, *Inorg. Chem.* **2009**, *48*, 4763 – 4767; b) J.-L. Chen, X.-D. Zhang, L.-Y. Zhang, L.-X. Shi, Z.-N. Chen, *Inorg. Chem.* **2005**, *44*, 1037 – 1043.

[22] a) C.-F. Lee, D. A. Leigh, R. G. Pritchard, D. Schultz, S. J. Teat, G. A. Timco, R. E. P. Winpenny, *Nature* **2009**, *458*, 314 – 318; b) E. C. Sanudo, T. B. Faust, C. A. Muryn, R. G. Pritchard, G. A. Timco, R. E. P. Winpenny, *Inorg. Chem.* **2009**, *48*, 9811 – 9818.

[23] a) Y.-f. Jiang, C.-j. Xi, Y.-z. Liu, J. Niclós-Gutiérrez, D. Choquesillo-Lazarte, *Eur. J. Inorg. Chem.* **2005**, 1585 – 1588; b) S. Tsuzuki, *Annu. Rep. Prog. Chem., Sect. C: Phys. Chem.* **2012**, *108*, 69 – 95; c) V. B. Medaković, M. K. Milčić, G. A. Bogdanović, S. D. Zarić, *J. Inorg. Biochem.* **2004**, *98*, 1867 – 1873.

[24] a) H. Ohtsu, J. Kitazume, T. Yamaguchi, *Dalton Trans.* **2011**, *40*, 7502 – 7504; b) F.-R. Dai, J.-L. Chen, H.-Y. Ye, L.-Y. Zhang, Z.-N. Chen, *Dalton Trans.* **2008**, 1492 – 1502.

[25] H.-Y. Ye, L.-Y. Zhang, J.-L. Chen, Z.-N. Chen, *Chem. Commun.* **2006**, 1971 – 1973.

[26] T. D. Goddard, D. G. Kneller, SPARKY 3, University of California, San Francisco.

[27] A. G. Palmer, III, J. Cavanagh, P. E. Wright, M. Rance, *J. Magn. Reson. Ser. A* **1991**, *93*, 151 – 170.

[28] A. Bax, D. G. Davis, *J. Magn. Reson. Ser. A* **1985**, *65*, 355 – 360.

[29] J. Jeener, B. H. Meier, P. Bachmann, R. R. Ernst, *J. Chem. Phys.* **1979**, *71*, 4546 – 4553.

[30] Gaussian 09, Revision A.02, M. J. Frisch, G. W. Trucks, H. B. Schlegel, G. E. Scuseria, M. A. Robb, J. R. Cheeseman, G. Scalmani, V. Barone, B. Mennucci, G. A. Petersson, H. Nakatsuji, M. Caricato, X. Li, H. P. Hratchian, A. F. Izmaylov, J. Bloino, G. Zheng, J. L. Sonnenberg, M. Hada, M. Ehara, K. Toyota, R. Fukuda, J. Hasegawa, M. Ishida, T. Nakajima, Y. Honda, O. Kitao, H. Nakai, T. Vreven, J. A. Montgomery, Jr., J. E. Peralta, F. Ogliaro, M. Bearpark, J. J. Heyd, E. Brothers, K. N. Kudin, V. N. Staroverov, R. Kobayashi, J. Normand, K. Raghavachari, A. Rendell, J. C. Burant, S. S. Iyengar, J. Tomasi, M. Cossi, N. Rega, J. M. Millam, M. Klene, J. E. Knox, J. B. Cross, V. Bakken, C. Adamo, J. Jaramillo, R. Gomperts, R. E. Stratmann, O. Yazyev, A. J. Austin, R. Cammi, C. Pomelli, J. W. Ochterski, R. L. Martin, K. Morokuma, V. G. Zakrzewski, G. A. Voth, P. Salvador, J. J. Dannenberg, S. Dapprich, A. D. Daniels, Ö. Farkas, J. B. Foresman, J. V. Ortiz, J. Cioslowski, D. J. Fox, Gaussian, Inc. Wallingford CT, **2009**..

[31] A. D. Becke, *J. Chem. Phys.* **1993**, *98*, 5648.

[32] a) X. Li, X. Liu, Z. Wu, H. Zhang, *J. Phys. Chem. A* **2008**, *112*, 11190; b) L. RodrÃguez, M. Ferrer, O. Rossell, F. J. S. Duarte, A. G. Santos, J. C. Lima, *J. Photochem. Photobiol. A* **2009**, *204*, 174; c) A. T. Radosevich, J. G. Melnick, S. A. Stoian, D. Bacciu, C.-H. Chen, B. M. Foxman, O. V. Ozerov, D. G. Nocera, *Inorg. Chem.* **2009**, *48*, 9214 – 9221.

[33] A. Schaefer, H. Horn, R. Ahlrichs, *J. Chem. Phys.* **1992**, *97*, 2571.

[34] L. Noodleman, D. A. Case, A. Aizman, *J. Am. Chem. Soc.* **1988**, *110*, 1001 – 1005.

[35] a) E. Cremades, J. Cano, E. Ruiz, G. Rajaraman, C. J. Milios, E. K. Brechin, *Inorg. Chem.* **2009**, *48*, 8012 – 8019; b) S. K. Singh, G. Rajaraman, *Dalton Trans.* **2013**, *42*, 3623 – 3630; c) F. Totti, G. Rajaraman, M. Iannuzzi, R. Sessoli, *J. Phys. Chem. C* **2013**, *117*, 7186 – 7190.

[36] G. Rajaraman, K. E. Christensen, F. K. Larsen, G. A. Timco, R. E. P. Winpenny, *Chem. Commun.* **2005**, 3053 – 3055.

[37] a) N. F. Chilton, R. P. Anderson, L. D. Turner, A. Soncini, K. S. Murray, *J. Comput. Chem.* **2013**, *34*, 1164 – 1175; b) A. Upadhyay, N. Komatireddy, A. Ghirri, F. Tuna, S. K. Langley, A. K. Srivastava, E. C. Sanudo, B. Moubaraki, K. S. Murray, E. J. L. McInnes, M. Affronte, M. Shanmugam, *Dalton Trans.* **2014**, *43*, 259 – 266.

Received: December 10, 2013
Published online on April 3, 2014

